

Improved Bandwidth of Patch Antenna Using Dual-Layer Metasurface

Kanglin Yang, Mingjiang Wang*, and Xiao Jia

School of Automation and Intelligence, Beijing Jiaotong University, Beijing 100044, China

ABSTRACT: A method for significantly improving the bandwidth of microstrip patch antennas is proposed, utilizing dual-layer metasurface (MS). The antenna employs coaxial probe feeding and consists of a truncated patch, an upper layer of 4×4 periodic N-shaped MS, and a lower layer of 3×4 rectangular MS. By introducing multiple resonances via dual-layer MSs, impedance matching of the patch antenna is greatly enhanced. Its overall geometric dimensions are $1.09\lambda_0 \times 1.09\lambda_0 \times 0.14\lambda_0$ ($f_0 = 5.5$ GHz), and compared with patch antennas and single-layer metasurface antennas of the same size, it can substantially enhance the bandwidth and gain without significant cost and size increase. The proposed MS antenna operates from 4.47 to 6.66 GHz (39.8% fractional bandwidth), covering two-thirds of the C-band, with a peak realized gain of 9.3 dBi. Within 4.47–5.56 GHz, the realized gain of the antenna remains above 7.5 dBi, and the average gain across the entire operating band is 7 dBi.

1. INTRODUCTION

Printed patch antennas are an important antenna type widely employed in modern wireless communication systems. They are characterized by compactness and light weight, making them suitable for integration into various communication devices and systems such as mobile phones and satellite communication equipment [1–3]. Additionally, their manufacturing process is relatively simple and cost-effective, facilitating mass production. Rectangular patch antennas are the most commonly used printed antennas, with their design parameters extensively analyzed [4, 5]. Traditional patch antennas typically exhibit narrow bandwidth ($< 5\%$). Researchers have employed various techniques to enhance the bandwidth of patch antennas, such as single-slot loading and multimode single-patch methods [6]. The former involves loading different forms of slots on the patch to generate new resonant frequencies, thereby increasing bandwidth [7]. The latter works by exciting more natural modes of the antenna through the feeding point, enabling the patch antenna to operate across multiple frequency bands simultaneously [8]. While these methods improve bandwidth to some extent, the operational bands are sometimes discrete, and gain enhancement is limited.

To address these issues, metasurface (MS) has been utilized to enhance the performance of patch antennas. MS is a new type of artificial material designed to achieve unique properties not typically found in nature [9]. It is usually placed above the antenna to manipulate the radiation behavior of electromagnetic waves [10–18]. Antennas based on MS are most commonly utilized to enhance bandwidth. In [10], the introduction of a dielectric metasurface (DMS) improved the fractional bandwidth and maximum realized gain of patch antenna by 12% and 6 dBi

at 2.45 GHz, respectively. A novel low-profile filtering antenna based on MS was proposed, achieving 20% fractional bandwidth and 8 dBi average realized gain [11]. In [12], the authors propose a circularly polarized antenna based on a rotating MS, achieving a fractional bandwidth of 47.9% and a peak realized gain of 7.75 dBi. In addition to bandwidth, MS antennas are also characterized by compactness, low profile, and high gain [13, 14]. Moreover, MS is also employed in the design of multi-band antennas. In [15], an MS-based decoupling method is proposed to reduce the mutual couplings at two independent bands of two coupled MIMO antennas. A dual-cap MS antenna is proposed in [16], operating at two WLAN frequency bands and exhibiting a peak gain of 7 dBi. In recent years, characteristic mode analysis (CMA) has been increasingly utilized in the design of MS. A high-gain, low-profile MS antenna was designed using CMA in [17], achieving a peak realized gain of 11.5 dBi with a thickness of only $0.11\lambda_0$. Ref. [18] employs CMA to elucidate the mechanism by which resonant apertures enhance the bandwidth of the proposed MS antenna.

Surface waves are generally considered detrimental in antenna application, as they cause strong coupling effects between patch elements in arrays, and numerous methods have been proposed to suppress their propagation [19]. Recently, surface waves have been introduced to enhance the performance of patch antennas. By loading a square metallic MS around the source patch, surface wave resonances are excited, significantly boosting the antenna's bandwidth and gain without increasing cost and volume. In [20], a patch antenna based on a single-layer MS provided 23.4% fractional bandwidth and 11 dBic peak realized gain in the millimeter-wave band. Square-ring antennas exploiting surface-wave MS achieved 27.4% fractional bandwidth and 11.9 dBi peak realized gain at 4.4 GHz [21].

* Corresponding author: Mingjiang Wang (mjwang@bjtu.edu.cn).

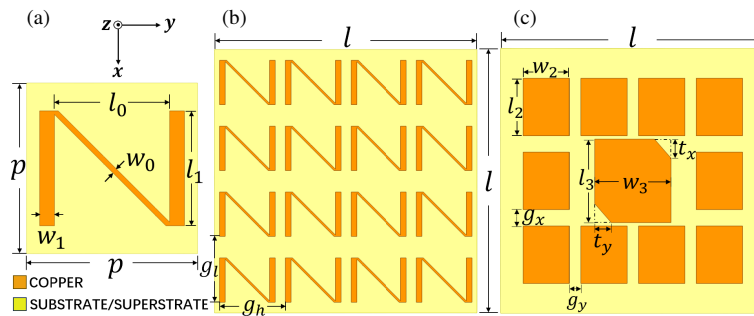


FIGURE 1. (a) Unit cell, (b) Upper MS, (c) Lower MS and source patch. The design parameters (in mm): $p = 15$, $l_0 = 10.1$, $w_0 = 0.46$, $l_1 = 10.1$, $w_1 = 1.3$, $l = 60$, $l_2 = 13.02$, $w_2 = 10.52$, $l_3 = 18.9$, $w_3 = 17$, $g_x = 3.71$, $g_y = 2.57$, $t_x = 4.29$, $t_y = 3.75$.

With the rapid development of wireless communications and the increasing number of channels, there is a growing demand for antennas with higher bandwidth. This letter proposes a dual-layer metasurface-based patch antenna that enhances antenna performance by exciting resonances in both upper and lower MS layers. Compared with single-layer MS antennas, it exploits the exposed portion of the substrate, thereby significantly enhancing bandwidth and gain without increasing volume or cost. The remainder of this letter is organized as follows. Section 2 provides a detailed description of the proposed antenna design and compares it with two other antenna types. Section 3 extensively analyzes proposed antenna's mechanism. In Section 4, simulated results are presented and compared. Finally, Section 5 draws conclusions.

2. DESIGN OF ANTENNA

Figure 1(a) shows the geometric structure of a single unit cell on upper-layer MS, where each unit cell is composed of microstrip lines and a substrate, with a periodicity p . The N-shaped microstrip lines consist of two vertical strips and a diagonal strip. The vertical strips have a length of l_1 and a width of w_1 , separated by l_0 . The diagonal strip has a width w_0 .

The upper-layer MS consists of 16 unit cells arranged in a 4×4 array. The spacing between any two lateral N-structures is given by $g_h = p - l_0 - 2w_1$, and the spacing between any two longitudinal N-structures is $g_l = p - l_1$, as depicted in Fig. 1(b). The lower-layer MS, illustrated in Fig. 1(c), comprises 10 rectangular metal patches arranged in a 3×4 configuration surrounding the source patch. Each patch has a length l_2 and a width w_2 . The spacing between the two rectangular patches along the x - and y -directions is denoted by g_x and g_y , respectively. Consequently, the periodicities of the patches in these two directions are $g_x + l_2$ and $g_y + w_2$. The source patch has a length l_3 and a width w_3 , with truncated lengths along the x and y axes of t_x and t_y . Both substrate and superstrate are square with side length l . Detailed parameters are provided in the caption of Fig. 1.

The proposed MS antenna utilizes coaxial probe feeding and comprises a truncated patch, upper and lower layers of MSs, air gap, and a ground plane. The center frequency is designed at 5.5 GHz. In order to demonstrate the effectiveness of the proposed structure, three configurations were exhibited in this section. Fig. 2 illustrates the design models of the three antennas.

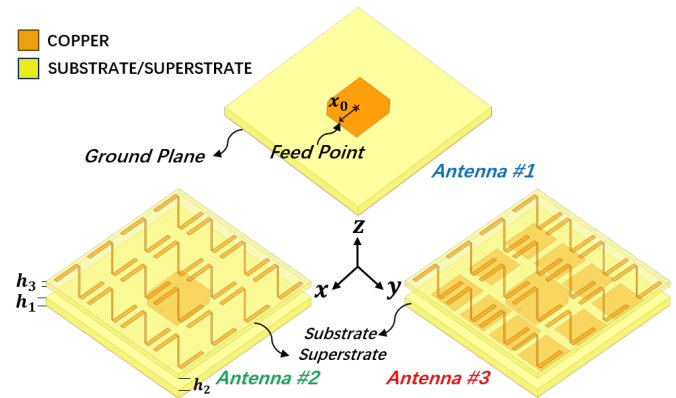


FIGURE 2. Three configurations of antenna models.

Ant. #1 is a conventional truncated rectangular patch antenna, cut in the shape of a not isosceles triangle. A 4×4 N-shaped MS is placed above Ant. #1 to excite additional resonances for bandwidth and gain enhancement in Ant. #2. Ant. #3, proposed in this letter, is loaded with additional rectangular metal patches around resource patch on the substrate to excite surface wave resonances. In addition, all the patches or microstrip lines of these antennas are printed on the top of substrate or superstrate. Substrate and superstrate use Rogers RT/Duroid5880 dielectric material ($\epsilon_r = 2.2$, $\tan \delta = 0.0009$). Other than differences in the models, all design parameters of these antennas are the same — e.g., thickness of substrate, overall size, and feeding mode. The design parameters in Fig. 2 include: the thicknesses of substrate and superstrate are $h_1 = 2.55$ mm and $h_3 = 1.5$ mm, respectively, and the thickness of the air layer between substrate and superstrate is $h_2 = 3.68$ mm. The distance from the feeding point to the center of the source patch is denoted as $x_0 = 8$ mm.

3. MECHANISM OF ANTENNA

3.1. Surface Wave of Lower Layer MS

In general, surface waves can exist in various geometric structures that include interfaces between medium. The discussion in this letter concerns the excitation of TM or TE surface waves on grounded dielectric substrates. The typical surface wave field refers to a field that exhibits exponential decay far from the medium surface but still retains a portion of the field preserved

near or within the medium. At higher frequencies, the field typically becomes more closely confined to the medium, thus the dielectric substrate can be considered as a waveguide [22]. In the proposed antenna, the lower layer MS is composed of periodically arranged rectangular metal patches. By loading MS around source patch on the substrate, the bandwidth is significantly improved due to the excitation of surface waves propagating along the MS to obtain extra resonances. Surface wave resonances are determined by the number of unit cells of MS and their periodicity, and can be determined along the x -direction by the following equation [23]:

$$\beta_{swx} L_{cav} = \pi \quad (1)$$

$$L_{cav} = P_x \times N_x \quad (2)$$

β_{swx} represents the propagation constant of the surface wave along x -direction; L_{cav} denotes the total length of MS cavity; P_x and N_x stand for the period and the number of unit cell along the x -direction, respectively.

We employ the dispersion mode method to analyze the periodic rectangular metal patches mentioned above and obtain the dispersion diagram. To generate the diagram, the solution type in HFSS is set to eigenmode. Subsequently, a unit cell model is constructed with periodic boundary conditions and perfect matching layer (PML), as depict in Fig. 3(a); corresponding parameters are provided in Fig. 1(c). Finally, parametric scans are conducted where parameters define the wave vector of the incident wave. k_x and k_y represent the wave number along the x and y -directions, respectively, traversing all possible incident wave vectors in the direction indicated by the arrows in Fig. 3(b) ($\Gamma \rightarrow X \rightarrow M \rightarrow \Gamma$, Brillouin zone), to determine the dispersion characteristics of the periodic structure.

The first two modes TM and TE are computed here. Drawing a vertical line representing solution of (1) on the dispersion

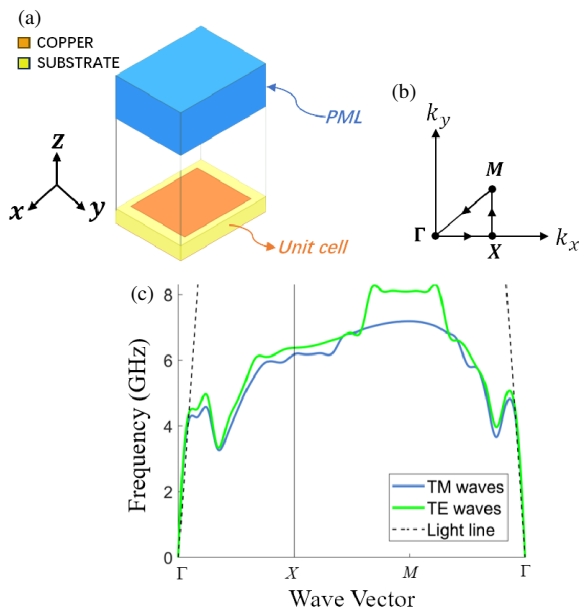


FIGURE 3. (a) Model of disperse pattern method for proposed configuration. (b) Wave vector definition of Brillouin zone. (c) Disperse diagram of proposed configuration.

diagram allows extraction of the surface wave resonance along the x -direction by intersecting with TM or TE mode curves, as shown in Fig. 3(c). For the proposed configuration, surface wave resonances are expected around 6.15 and 6.36 GHz.

Electric field distributions of proposed antenna on the substrate's xz -plane are calculated at 5, 5.5, 6.25, and 6.5 GHz. In Fig. 4(a), it can be observed that at 5 GHz, a small portion of the electric field energy concentrates at the center of the substrate. However, at 6.25 and 6.5 GHz, surface waves are excited, with the electric field intensity exhibiting a distinct sinusoidal distribution as depicted in Figs. 4(c) and (d). Therefore, there exist surface wave resonances near these two frequencies. This is not completely consistent with the results obtained in Fig. 3. Because Fig. 3 analyzes a single unit cell, while Fig. 4 presents the full-wave simulation results for the proposed antenna.

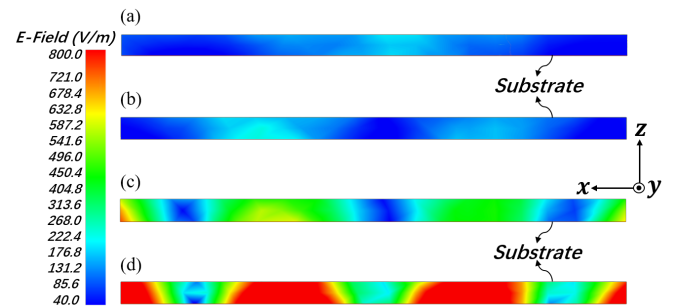


FIGURE 4. Magnitude of electric fields (a) at 5 GHz and (b) at 5.5 GHz, (c) at 6.25 GHz, (d) at 6.5 GHz on the substrate's xz -plane.

3.2. Effective Parameters of Upper Layer MS

As mentioned in Section 2, with the addition of upper layer N-shaped MS, Ant. #2 can excite extra resonances, resulting in improved bandwidth and realized gain compared to Ant. #1. Next, the mechanism will be explained. In HFSS, the unit cell is excited under periodic boundary conditions to simulate an infinite MS structure, with excitation applied via Floquet ports as depicted in Fig. 5. The parameters of the unit cell are provided in Fig. 1(a). Port 1 serves as the incident port. This approach allows us to study primitive electromagnetic properties of the N-shaped MS.

According to effective-medium theory, the electromagnetic parameters of MS, such as effective permeability and permittivity, can be retrieved from scattering coefficients [24]. However, in this approach, the thickness of the equivalent layer d is not uniquely defined, leading to ambiguities in the retrieved parameters as they depend on the chosen d value. Therefore, we adopt a method based on Generalized Sheet Transition Conditions (GSTCs) to retrieve the electromagnetic parameters of MS [25]. This method, compared to effective-medium theory, is more suitable for describing MS, where the electromagnetic properties are characterized by uniquely determined surface electric susceptibility $\vec{\chi}_{ES}$ and surface magnetic susceptibility $\vec{\chi}_{MS}$ in [26]:

$$\vec{\chi}_{ES} = \chi_{ES}^{xx} \mathbf{a}x\mathbf{a}x + \chi_{ES}^{yy} \mathbf{a}y\mathbf{a}y + \chi_{ES}^{zz} \mathbf{a}z\mathbf{a}z \quad (3)$$

$$\vec{\chi}_{MS} = \chi_{MS}^{xx} \mathbf{a}x\mathbf{a}x + \chi_{MS}^{yy} \mathbf{a}y\mathbf{a}y + \chi_{MS}^{zz} \mathbf{a}z\mathbf{a}z \quad (4)$$

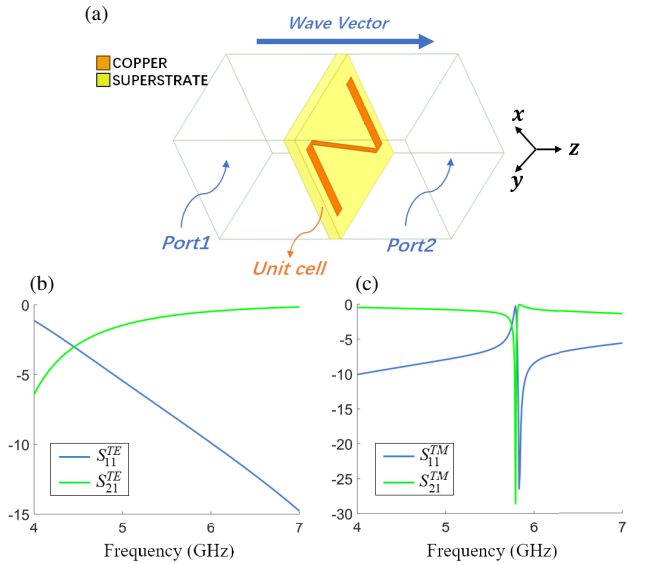


FIGURE 5. (a) Unit cell of upper layer MS. (b) S_{11}^{TE} and S_{21}^{TE} . (c) S_{11}^{TM} and S_{21}^{TM} .

for TE polarized normal incident wave, two surface susceptibilities components are determined by the following formula:

$$\chi_{MS}^{xx} = -\frac{2j S_{11}^{TE} - S_{21}^{TE} + 1}{k_0 S_{11}^{TE} - S_{21}^{TE} - 1} \quad (5)$$

$$\chi_{ES}^{yy} = \frac{2j S_{11}^{TE} + S_{21}^{TE} - 1}{k_0 S_{11}^{TE} + S_{21}^{TE} + 1} \quad (6)$$

similarly, for TM polarized normal incident wave, the two components are determined by the following:

$$\chi_{ES}^{xx} = -\frac{2j S_{11}^{TM} - S_{21}^{TM} + 1}{k_0 S_{11}^{TM} - S_{21}^{TM} - 1} \quad (7)$$

$$\chi_{MS}^{yy} = \frac{2j S_{11}^{TM} + S_{21}^{TM} - 1}{k_0 S_{11}^{TM} + S_{21}^{TM} + 1} \quad (8)$$

where k_0 represents the wave number in vacuum; S_{11}^{TE} and S_{21}^{TE} denote the reflection coefficient and transmission coefficient under TE polarization, respectively. S_{11}^{TM} and S_{21}^{TM} are the same. Since we are discussing planar structures here, components along the z -direction are not considered. Upon obtaining the scattering coefficients, the retrieved parameters versus frequency are shown in Figs. 6(a)–(d). From Fig. 6(a), it can be observed that the surface magnetic susceptibility is negative within the 4–4.7 GHz range, indicating strong diamagnetic behavior of the MS in this frequency band. Diamagnetic MS is considered a cost-effective solution due to its straightforward planar structure [10, 27]. The gain improvement of Ant. #2 can be explained due to the diamagnetic property which gives a low refractive index from the MS, according to Snell’s law of refraction. Furthermore, from Fig. 6, it is evident that for both TE and TM polarized incident waves, the MS exhibits sharp changes in surface electric and magnetic susceptibilities at certain frequencies. For a complete system composed of MS and

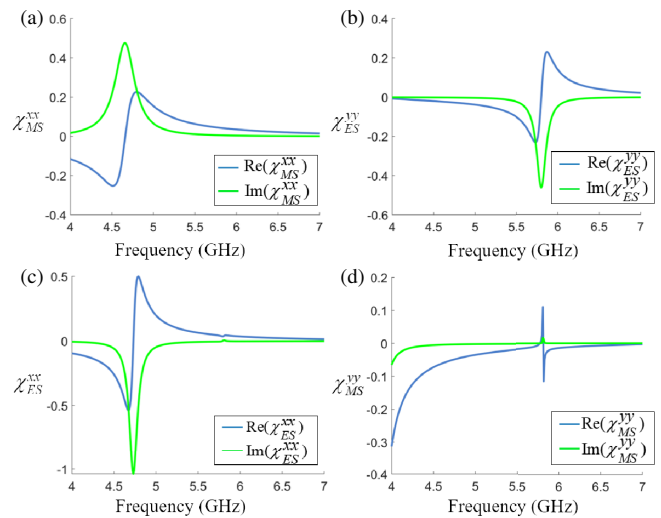


FIGURE 6. (a) and (b) Surface susceptibilities of TE polarized incident wave, (c) and (d) Surface susceptibilities of TM polarized incident wave.

antennas, from circuit theory, this signifies abrupt changes in impedance at certain frequencies, thereby causing variations in resonance frequencies.

4. SIMULATED RESULTS AND COMPARISON

This letter employs ANSYS HFSS to perform full-wave simulations on the three antennas mentioned above. The simulation results are detailed in Figs. 7(a) and (b). The resonance of Ant. #1 occurs at 5.35 GHz, at which frequency it achieves a maximum gain of 8.25 dBi. Its return loss bandwidth (RLBW) is only 6.2%. Ant. #2 yields two resonances at 5.35 and 5.55 GHz, with the latter induced by the upper layer MS. Consequently, its RLBW is increased to 17.3% (4.99–5.94 GHz), with a peak gain of 8.53 dBi at 5.15 GHz. After the addition of the lower layer MS to excite surface wave resonances, Ant. #3 exhibits four resonant points within the bandwidth, significantly enhancing the antenna performance: the RLBW is 39.8% (4.47–6.66 GHz), with a peak realized gain of 9.3 dBi at 4.94 GHz and an average in-band gain of 7 dBi. Its realized gain remains above 7.5 dBi within 4.47–5.56 GHz. The mechanisms behind these phenomena have been discussed in detail in Section 3.

In the frequency band of 5.5–6.5 GHz, oscillation in realized gain was observed. As shown in Fig. 7(a), compared to Ant. #2, the addition of the lower layer MS to Ant. #3 introduced two additional resonance frequencies, and the two minima in the realized gain curve in Fig. 7(b) occur near these frequencies. The purpose of adding the lower layer MS is to excite surface wave resonance, and thus, the two extra resonance frequencies are generated by the excitation of surface waves. According to Fig. 4(a), when surface waves are not excited, only a small portion of the energy is concentrated at the center of the substrate. Therefore, most of the energy is radiated from the source patch (Ant. #1) and is relatively concentrated. However, by observing Figs. 4(c) and (d), it is evident that when surface waves are excited, the energy distribution exhibits a pronounced sinusoidal pattern with higher intensity. This indicates that less

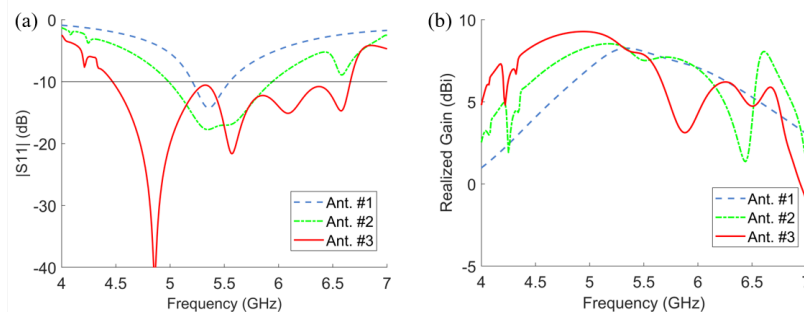


FIGURE 7. (a) Simulated $|S_{11}|$ and (b) broadside realized gain ($\theta = 0^\circ, \varphi = 0^\circ$) in different configurations shown in Fig. 2.

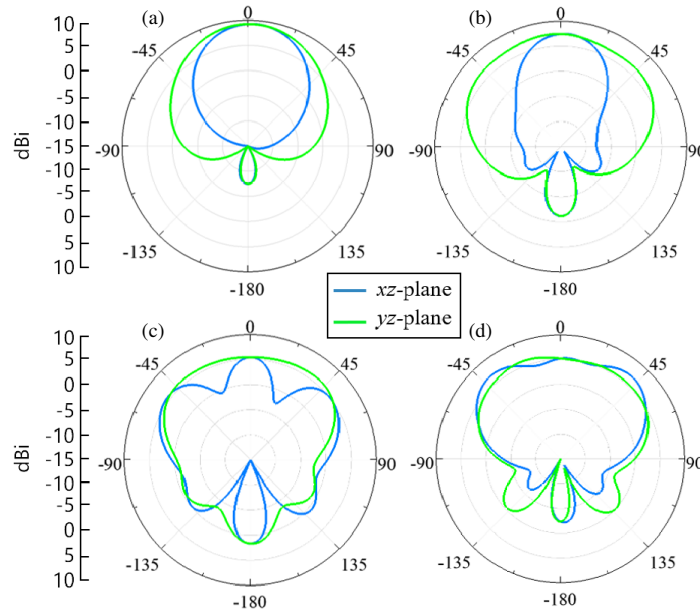


FIGURE 8. Radiation patterns of the proposed antenna (Ant. #3) at xz - and yz -planes, (a) at 4.86 GHz, (b) at 5.57 GHz, (c) at 6.1 GHz, (d) at 6.58 GHz.

TABLE 1. Comparison of simulated results between proposed antenna and high-performance antennas.

Antenna structures	Center frequency (GHz)	Size (λ_0^3)	-10 dB RLBW (%)	Peak Gain (dBi)
Ref. [12]	6.2	$0.67 \times 0.67 \times 0.06$	46.7	7.7
Ref. [13]	10.44	$0.9 \times 0.9 \times 0.29$	11.54	9.3
Ref. [14]	5	$0.65 \times 0.65 \times 0.067$	20	N/A
Ref. [17]	5.8	$1.5 \times 0.83 \times 0.11$	6.84	12
Ref. [18]	4.8	$1 \times 1 \times 0.058$	25	10.3
Ref. [21]	4.5	$1.13 \times 1.13 \times 0.07$	27.27	11.9
Prop.	5.5	$1.09 \times 1.09 \times 0.14$	39.8	9.3

energy is directly radiated from the source patch, and instead, energy is radiated from the entire substrate. Compared to the scenario without surface wave excitation, the energy radiated in this case is more dispersed, leading to the two minima in the gain curve shown in Fig. 7(b). The above analysis can also be verified by comparing (a), (b) and (c), (d) in Fig. 8.

Figure 8 shows the simulated total radiation pattern in the xz - and yz -planes at four resonant frequencies. Nearly symmetrical radiation patterns are viewed.

Table 1 provides a comparison of simulation performance between the proposed antenna and some reported high-performance antennas.

5. CONCLUSION

In this study, a broadband, single-feed, dual-layer metasurface-based microstrip patch antenna is designed and analyzed. Compared to conventional patch antennas, significant improvements are achieved in terms of Return Loss Bandwidth (RLBW) and realized gain. The lower layer MS excites surface waves, while the upper layer MS adjusts impedance matching of the system. Dispersion diagrams are employed to analyze surface wave resonance of the lower layer MS, and surface electric and magnetic susceptibilities is used to characterize the electromagnetic properties of the upper layer MS. The obtained results are consistent with simulation. The proposed antenna has an overall size of $1.09\lambda_0 \times 1.09\lambda_0 \times 0.14\lambda_0$ with a low profile, suitable for various miniaturized applications. The proposed technique capitalizes on the exposed space around the source patch without expanding the antenna's volume, with manufacturing costs remaining virtually unchanged. Operating in the C-band, it achieves a fractional bandwidth of 39.8%, with a peak realized gain of 9.3 dBi, making it highly suitable for wide-ranging applications in base station antennas and satellite terminal equipment.

ACKNOWLEDGEMENT

This work is supported by the Fundamental Research Funds for the Central University under the Grant of KAIJBM24001536 and the Red Orchard Project of Beijing Jiaotong University with Grant KAIGY24007530.

REFERENCES

- [1] Rana, M. S. and M. M. R. Smiee, "Design and analysis of microstrip patch antenna for 5G wireless communication systems," *Bulletin of Electrical Engineering and Informatics*, Vol. 11, No. 6, 3329–3337, Dec. 2022.
- [2] Lin, S.-Y. and K.-C. Huang, "A compact microstrip antenna for GPS and DCS application," *IEEE Transactions on Antennas and Propagation*, Vol. 53, No. 3, 1227–1229, Mar. 2005.
- [3] Patel, D. H. and G. D. Makwana, "A comprehensive review on multi-band microstrip patch antenna comprising 5G wireless communication," *International Journal of Computing and Digital Systems*, Vol. 11, No. 1, 941–953, Feb. 2022.
- [4] Derneryd, A., "A theoretical investigation of the rectangular microstrip antenna element," *IEEE Transactions on Antennas and Propagation*, Vol. 26, No. 4, 532–535, Jul. 1978.
- [5] Kara, M., "Closed-form expressions for the resonant frequency of rectangular microstrip antenna elements with thick substrates," *Microwave and Optical Technology Letters*, Vol. 12, No. 3, 131–136, Jun. 1996.
- [6] Kumar, G. and K. P. Ray, *Broadband Microstrip Antennas*, Artech House, Dedham, MA, 2002.
- [7] Lam, K. Y., K.-M. Luk, K. F. Lee, H. Wong, and K. B. Ng, "Small circularly polarized U-slot wideband patch antenna," *IEEE Antennas and Wireless Propagation Letters*, Vol. 10, 87–90, Feb. 2011.
- [8] Liu, N.-W., X.-P. Chen, L. Zhu, X. Chen, G. Fu, and Y. Liu, "Low-profile triple-band microstrip antenna via sharing a single multi-mode patch resonator," *IET Microwaves, Antennas & Propagation*, Vol. 13, No. 10, 1580–1585, 2019.
- [9] Holloway, C. L., E. F. Kuester, J. A. Gordon, J. O'Hara, J. Booth, and D. R. Smith, "An overview of the theory and applications of metasurfaces: The two-dimensional equivalents of metamaterials," *IEEE Antennas and Propagation Magazine*, Vol. 54, No. 2, 10–35, Apr. 2012.
- [10] Chung, K. L. and S. Chaimool, "Diamagnetic metasurfaces for performance enhancement of microstrip patch antennas," in *Proceedings of the 5th European Conference on Antennas and Propagation (EUCAP)*, 48–52, Rome, Italy, 2011.
- [11] Yang, W., S. Chen, Q. Xue, W. Che, G. Shen, and W. Feng, "Novel filtering method based on metasurface antenna and its application for wideband high-gain filtering antenna with low profile," *IEEE Transactions on Antennas and Propagation*, Vol. 67, No. 3, 1535–1544, Mar. 2019.
- [12] Qu, X., R. Bai, P. Wang, M. Li, Z. Zhang, S. Xiao, C. Li, and G. Zhu, "A single-fed broadband circularly polarized antenna based on rotating metasurface," *Progress In Electromagnetics Research C*, Vol. 146, 119–126, 2024.
- [13] Samantaray, D. and S. Bhattacharyya, "A gain-enhanced slotted patch antenna using metasurface as superstrate configuration," *IEEE Transactions on Antennas and Propagation*, Vol. 68, No. 9, 6548–6556, Sep. 2020.
- [14] Li, W., Y. M. Wang, Y. Hei, B. Li, and X. Shi, "A compact low-profile reconfigurable metasurface antenna with polarization and pattern diversities," *IEEE Antennas and Wireless Propagation Letters*, Vol. 20, No. 7, 1170–1174, Jul. 2021.
- [15] Liu, F., J. Guo, L. Zhao, G.-L. Huang, Y. Li, and Y. Yin, "Dual-band metasurface-based decoupling method for two closely packed dual-band antennas," *IEEE Transactions on Antennas and Propagation*, Vol. 68, No. 1, 552–557, Jan. 2020.
- [16] Chen, X. and H. Dou, "Compact dual-band antenna based on dual-cap metasurface," *Progress In Electromagnetics Research M*, Vol. 128, 11–20, 2024.
- [17] Wang, K., W. Shao, X. Ding, B.-Z. Wang, and B. Jiang, "Design of high-gain metasurface antenna based on characteristic mode analysis," *IEEE Antennas and Wireless Propagation Letters*, Vol. 21, No. 4, 661–665, Apr. 2022.
- [18] Lin, F. H. and Z. N. Chen, "Resonant metasurface antennas with resonant apertures: Characteristic mode analysis and dual-polarized broadband low-profile design," *IEEE Transactions on Antennas and Propagation*, Vol. 69, No. 6, 3512–3516, Jun. 2021.
- [19] Yang, F. and Y. Rahmat-Samii, "Microstrip antennas integrated with electromagnetic band-gap (EBG) structures: A low mutual coupling design for array applications," *IEEE Transactions on Antennas and Propagation*, Vol. 51, No. 10, 2936–2946, Oct. 2003.
- [20] Hussain, N., M.-J. Jeong, A. Abbas, and N. Kim, "Metasurface-based single-layer wideband circularly polarized MIMO antenna for 5G millimeter-wave systems," *IEEE Access*, Vol. 8, 130 293–130 304, Jul. 2020.
- [21] Alharbi, M. S., C. A. Balanis, and C. R. Birtcher, "Performance enhancement of square-ring antennas exploiting surface-wave metasurfaces," *IEEE Antennas and Wireless Propagation Letters*, Vol. 18, No. 10, 1991–1995, Oct. 2019.
- [22] Pozar, D. M., *Microwave Engineering*, Publishing-House-of-Electronics-Industry, NJ, USA, 2006.
- [23] Costa, F., O. Luukkonen, C. R. Simovski, A. Monorchio, S. A. Tretyakov, and P. M. de Maagt, "Te surface wave resonances on high-impedance surface based antennas: Analysis and modeling," *IEEE Transactions on Antennas and Propagation*, Vol. 59, No. 10, 3588–3596, Oct. 2011.

- [24] Chen, X., T. M. Grzegorzczak, B.-I. Wu, J. Pacheco, and J. A. Kong, "Robust method to retrieve the constitutive effective parameters of metamaterials," *Physical Review E*, Vol. 70, No. 1, 016608, 2004.
- [25] Holloway, C. L., A. Dienstfrey, E. F. Kuester, J. F. O'Hara, A. K. Azad, and A. J. Taylor, "A discussion on the interpretation and characterization of metafilms/metasurfaces: The two-dimensional equivalent of metamaterials," *Metamaterials*, Vol. 3, No. 2, 100–112, 2009.
- [26] Kuester, E. F., M. A. Mohamed, M. Piket-May, and C. L. Holloway, "Averaged transition conditions for electromagnetic fields at a metafilm," *IEEE Transactions on Antennas and Propagation*, Vol. 51, No. 10, 2641–2651, Oct. 2003.
- [27] Economou, E. N., T. Koschny, and C. M. Soukoulis, "Strong diamagnetic response in split-ring-resonator metamaterials: Numerical study and two-loop model," *Physical Review B*, Vol. 77, No. 9, 092401, 2008.